Supporting Information: Shortwave and longwave radiative contributions to global warming under increasing CO_2

Aaron Donohoe [*], **Kyle C. Armour** [*], **Angeline G. Pendergrass** [†] **and David S. Battisti** [‡]

[*]Department of Earth, Atmospheric and Planetary Sciences, Massachusetts Institute of Technology, Cambridge, MA, USA, [†]National Center for Atmospheric Research, Boulder, CO, USA, and [‡]Department of Atmospheric Sciences, University of Washington, Seattle, WA, USA

Submitted to Proceedings of the National Academy of Sciences of the United States of America

Here, we derive the analytical solutions to the OLR recovery time in response to an instantaneous and linearly increasing GHG forcing (τ_{cross} in Eq. [6] and τ_{ramp} in Eq. [8]). We also elaborate on the observational calculations of the linear feedback parameters (λ_{SW} and λ_{LW}) and the climate system heat capacity (C).

Derivation of Eqs. [6] and [8]

The time evolution of global mean surface temperature from the solution of Eq. [1] under an instantaneous greenhouse forcing and with a time-invariant C is

$$T_S = \frac{F_{LW} + F_{SW}}{\lambda_{LW} + \lambda_{SW}} \left(e^{\frac{-t}{\tau}} - 1 \right). \qquad [\mathbf{A\text{-}1}]$$

The time evolution of the OLR is found by substituting Eq. [**A-1**] into Eq. [2]:

$$OLR(t) = -F_{LW} + \frac{(F_{LW} + F_{SW})\,\lambda_{LW}}{\lambda_{LW} + \lambda_{SW}} \left(1 - e^{\frac{t}{\tau}} \right) \qquad [\mathbf{A\text{-}2a}]$$

$$= -F_{LW} + F_{LW} \left[\underbrace{\left(1 + \frac{F_{SW}}{F_{LW}} \right)}_{G_{F_{SW}}} \underbrace{\left(\frac{1}{1 + \frac{\lambda_{SW}}{\lambda_{LW}}} \right)}_{G_{\lambda_{SW}}} \right] \left(1 - e^{\frac{t}{\tau}} \right). \qquad [\mathbf{A\text{-}2b}]$$

Identifying OLR(t=τ_{cross}) = 0 in Eq. [**A-2b**] and solving for τ_{cross} gives Eq. [6] of the text.

The ramped forcing in the 1%CO_2 runs can be thought of as the summation of many heaviside functions each starting at a different time step, in the limit that the step size goes to zero. Therefore, the surface temperature response to a ramped forcing in the linear feedback model is equal to the sum of the responses to an instantaneous forcing (Eq. [**A-1**]) each starting at a different time after the forcing has started:

$$T_{S,ramp} = \int_0^t \frac{dF}{dt} \frac{1 - e^{\frac{-t}{\tau}}}{-(\lambda_{LW} + \lambda_{SW})} dt \qquad [\mathbf{A\text{-}3a}]$$

$$= \frac{\dot{F}}{-(\lambda_{LW} + \lambda_{SW})} \left(\underbrace{t - \tau}_{steady} + \underbrace{\tau e^{\frac{-t}{\tau}}}_{transient} \right) \qquad [\mathbf{A\text{-}3b}]$$

as shown by Kim et al. [1]. $\dot{F}$ is the time derivative of the forcing which is constant in this experiment. The first term in Equation [**A-3b**] represents the long term response to the ramped forcing in which the temperature increases linearly in time and the second term represents the transient response which decays on the same e-folding time scale found in the analysis of the 4×CO_2 runs. We note that the long term temperature change is *not* equal to the time integrated forcing divided by the feedback (as is the case for the equilibrium response to instantaneous forcing), but is offset from this solution by the equivalent of τ years of integrated forcing. In this case, the TOA energy balance is never achieved but rather, the TOA energy *imbalance* becomes constant in time and drives a constant surface temperature tendency (surface temperature increases linearly in time) such that $\dot{F}$ is balanced by the surface temperature tendency times the sum of the feedback parameters. We note that after several e-folding timescales (> 50 years) the system nearly asymptotes to the steady linear increase.

The time evolution of the OLR can be found by substituting Equation [**A-3b**] into Equation [2]:

$$OLR_{RAMP}(t) = -\dot{F}_{LW} t + \qquad [\mathbf{A\text{-}4a}]$$

$$\frac{\lambda_{LW}}{\lambda_{LW} + \lambda_{SW}} \left(\dot{F}_{LW} + \dot{F}_{SW} \right) \left(t - \tau + \tau e^{\frac{-t}{\tau}} \right) \qquad [\mathbf{A\text{-}4b}]$$

$$\approx \dot{F}_{LW} t \left(G_{F_{SW}}\, G_{\lambda_{SW}} \left(1 - \frac{\tau}{t} \right) - 1 \right), \qquad [\mathbf{A\text{-}4c}]$$

where we have ignored the transient term in the approximation. Identifying t=τ_{ramp} when the left hand side of Equation [**A-4c**] = 0 and solving for τ_{ramp} gives Eq. [10].

Observational estimates of λ_{SW} and λ_{LW}

The co-variability of the global mean, forcing adjusted ASR and OLR with the global average surface temperature is used to estimate λ_{SW} and λ_{LW}. Radiation data are from the Clouds and the Earth's Radiant Energy System Energy Balanced and Filled product(CERES EBAF) [2] and span the period 2000-2013. Monthly anomalies are used, since the seasonal cycle of reflected SW is primarily due to the spatial distribution of insolation and planetary albedo [3] and is, thus, not a consequence of radiative feedbacks. Insolation variability

Reserved for Publication Footnotes

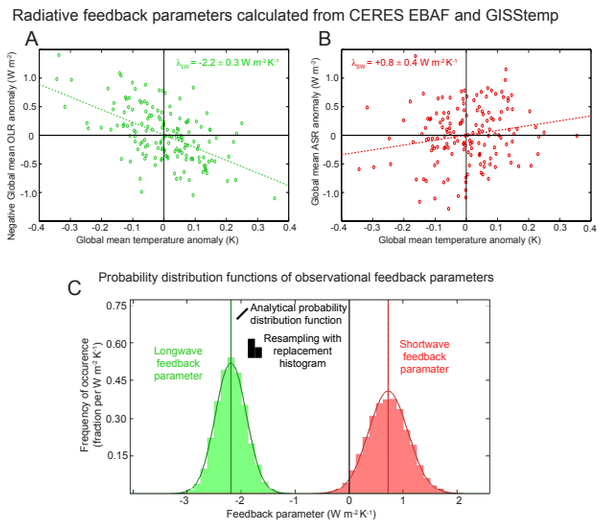

Fig. 1. (A) Scatter plot of the (forcing adjusted) anomaly in net LW radiation at TOA (negative OLR) from CERES EBAF and the global mean surface temperature anomaly from GISTEMP. The circles are monthly anomalies from climatology (2000-2013) and the dashed line is the linear best fit with slope equal to λ_{LW} (the value and uncertainty is shown in the panel). (B) As in (A) except for ASR (ordinate) with the resulting estimate of λ_{SW}. (C) Histogram of observational feedback parameters calculated from a 10,000 member (bootstraped) Monte-Carlo re-sampling of the CERES EBAF radiation data and GISTEMP temperature data (shaded blocks). LW estimates are shown in green and SW estimates are shown in red. The solid lines are the analytical probability distribution function derived from the full record (equation [**A-6**] and [**A-7**]). The mean of the Monte-Carlo estimate is shown by the dashed vertical line and the regression coefficient derived from the full record is shown by the solid vertical line (the lines lie on top of one another).

(global mean $2\sigma = 0.2$ W m^{-2}) is removed from the CERES EBAF data since this leads to variations in TOA radiation that are externally forced and unrelated to climate feedbacks. The impact of insolation anomalies on the reflected shortwave radiation is also removed by subtracting the anomalous insolation times the climatological planetary albedo from the upwelling SW. This method is equivalent to calculating anomalies in planetary albedo and multiplying by the climatological insolation to convert to W m^{-2}.

We calculate the observed SW forcing due to stratospheric aerosols and the observed LW forcing associated with increased greenhouse gases as follows. The inter-annual variability of stratospheric aerosol forcing is calculated from Solomon et al.'s [4] aerosol optical depth which uses combined satellite observations from the Stratospheric Aerosol and Gas Experiment (SAGE) II (1990 to 2005), Global Ozone Monitoring by Occulation of Stars (GOMOS, 2002 to 2009), and the CALIPSO lidar (2006 to 2010) to produce a continuous record of aerosol optical depth above 15 km between 50S and 50N. We convert the aerosol optical depth to TOA SW forcing using a conversion factor of 25 W m^{-2} [5]. Greenhouse gas forcing is calculated separately for CO_2, CH_4 and N_2O. Monthly, global mean CO_2 concentrations from the NOAA Earth System Research Laboratory [6] are converted to radiative forcing using

$$F_{LW_{CO_2}} = 5.57 Wm^{-2} \ln\left(\frac{CO_2}{CO_{2,REF}}\right), \qquad [\mathbf{A\text{-}5}]$$

where $CO_{2,REF}$ is the reference concentration, taken here as the time average over the analysis period. CH_4 and N_2O forcing are taken from the NOAA Annual Greenhouse Gas Index (http://www.esrl.noaa.gov/gmd/aggi/aggi.html). The annual mean radiative forcing data are linearly interpolated to monthly resolution. The greenhouse gas forcings are converted to anomalies over the observational period and are subtracted from the global mean OLR anomalies prior to our analysis of the feedback factor λ_{LW}.

Three different sets of surface temperature data are considered here: 1. NCEP reanalysis surface air temperature [7], 2.the Goddard Institute for Space Studies Surface Temperature Analysis (GISTEMP)[8] and 3. Cowtan and Way's modification [9] of the Met Office Hadley Centre's surface temperature data set ([10]). All data are converted to anomalies from the climatological annual cycle over the period 2000-2013. Gridpoints with missing data at any time over the analysis period are excluded. We use globally (spatially weighted) averaged data in our analyses. In all three data sets, the global average temperature exhibits a significant (95% confidence interval) upward trend. The amplitude of the trend – quantified by the regression coefficient times half of the 13 years analysis period– is 0.08,0.02 and 0.07 K for the NCEP, GISTEMP and Hadley Centre data, respectively. The amplitude of the detrended, monthly and globally averaged temperature (2σ) is 0.28, 0.22 and 0.25 K in the NCEP, GISTEMP and Hadley Centre data. In all cases, the amplitude of variability in the detrended data exceeds the amplitude associated with the trend; the inter-annual variability of global average temperature exceeds the global warming signal associated with increasing greenhouse gases over the 13 year analysis period. We note that, we do *not* detrend the data prior to our analysis as the signals we wish to capture are the radiation changes as the planet warms (either due to global warming or internal variability).

The regression slope between global averaged OLR and global averaged surface temperature anomalies, which we equate with λ_{LW}, ranges from -2.2 ± 0.3 W m^{-2} K^{-1} (uncertainty is 1σ) with the GISTEMP data (Fig. S1A) to -1.7 ± 0.2 W m^{-2} K^{-1}with the NCEP reanalysis surface temperature data (Table 1). For all three temperature data sets, the net shortwave radiation at the TOA (forcing and insolation adjusted) increases with global mean temperature, consistent with the positive SW feedback found previously [11]. We find λ_{SW} to be $+0.8 \pm 0.4$, $+0.7 \pm 0.4$ and $+0.9 \pm 0.4$ W m^{-2} K^{-1} using the GISTEMP (Fig. S1B), NCEP reanalysis and Hadley Centre temperature data, respectively. Averaging across all three analyses yields $\lambda_{SW} = +0.8 \pm 0.4$ W m^{-2} K^{-1} and $\lambda_{LW} = -2.0 \pm 0.4$ W m^{-2} K^{-1} . These values place the shortwave feedback within the range spanned by the CMIP5 models but somewhat greater than the ensemble average λ_{SW} of +0.6 W m^{-2} K^{-1}. The observed longwave feedback is slightly more stabilizing than the CMIP5 models' ensemble average λ_{LW} of -1.7 W m^{-2} K^{-1}.

For all three temperature data sets, correlation between temperature and each of the radiation components is significant at the 99% confidence interval despite the small fraction of variance explained (r^2 averages 0.28 for OLR and 0.05 for ASR). The uncertainity in the feeback parameters (σ_λ) is estimated by way of the standard deviation of each time series σ, the correlation coefficient between the time series r, and the degrees of freedom N^* using the approximation[12]:

$$\sigma_{\lambda_{SW}} = \frac{\sigma_{ASR}\sqrt{1 - r^2_{ASR,T_S}}}{\sigma_{T_S}\sqrt{N^*}}, \qquad [\mathbf{A\text{-}6}]$$

A similar expression holds for the uncertainty in λ_{LW} with ASR replaced by OLR. The degrees of freedom (N*) are calculated from the lag one month autocorrelation, r(Δt), of T$_S$

and OLR/ASR and the number of months in the record (N) [13]:

$$N^* = N\frac{1 - r(\Delta t)_{T_S}\, r(\Delta t)_{ASR}}{1 + r(\Delta t)_{T_S}\, r(\Delta t)_{ASR}}. \qquad [\mathbf{A\text{-}7}]$$

The one month lag autocorrelation of T_S ($r(\Delta t)_{T_S}$), averaged over the three temperature data sets, is 0.61. The one month lag autocorrelation in ASR and OLR is significantly lower (0.10 and 0.31, respectively). As a result, the effective degrees of freedom in the 160 month record used to calculate the regression of temperature with ASR is $N^* = 143$ while that for temperature with OLR is $N^* = 113$. Eq. [**A-6**] lends insight into why the error bounds (σ_λ) on λ_{SW} and λ_{LW} are relatively small despite the weak correlation between the TOA radiation and the surface temperature. In the limiting case of no physical relationship between ASR and T_S, one would expect a regression coefficient of zero with some variation due to random chance correlations within the sample realized. The maximum possible regression is equal to $\sigma_{ASR}/\sigma_{T_S} = 4$ W m^{-2} K^{-1} which would be realized if the variables were perfectly correlated, in this hypothetical example by random chance. Random correlations are less likely with larger samples and, thus, the regression coefficient converges to its true value as the sample size increases. In our case, with on the order of 100 independent data, it is unlikely (1σ) to get a random correlation coefficient that exceeds 0.1 ($1/\sqrt{N^*}$) in magnitude. Therefore, the regression coefficient due to random noise should not exceed (4 W m^{-2} K^{-1}/10 =) 0.4 W m^{-2} K^{-1}. Hence, the calculated λ_{SW} of 0.8 W m^{-2} K^{-1} is statistically significant. The feedback parameters are statistically significant because it is highly unlikely to find values of this magnitude in the absence of a true feedback process even if processes other than temperature feedbacks make a larger contribution to the TOA radiation variance. To further see this point, we randomly sub-sample the surface temperature and TOA radiation data and create 10,000 estimates of the feedback parameters using a (bootstrapped) Monte-Carlo simulation. For each estimate, we create a time series of each data set with 160 monthly values by randomly sampling the full data set with replacement. The resulting probability distribution function for λ_{SW} and λ_{LW} agrees very well with that expected from Eq. [**A-6**] (Fig. S1C). We emphasize that it is highly unlikely that $\lambda_{SW} < 0$; fewer than 1% of the Monte-Carlo realizations give negative values for λ_{SW}.

Observational estimate of climate system heat capacity

Here, we estimate the heat capacity of the climate system from observations for the period 1970 - 2012. As defined by Eq. [1], the heat capacity is the time integrated global energy accumulation divided by the resulting global mean surface temperature change. The changes in the energy content of the atmospheric column, land surface, and cryosphere are negligible compared with the changes in energy content in the ocean. Hence, the time integrated energy accumulation in the climate system is equal to the ocean heat content anomaly. The latter is provided by data from the World Ocean Atlas [14](Fig. S2A). The regression coefficient between ocean heat content anomalies (relative to the 1970-2012 period) and global mean surface temperature anomalies from NCEP reanalysis, GISTEMP and the Hadley Centre gives three estimates of the climate system heat capacity, C. These values range from 10 $\pm$2 to 14 $\pm$3 W m^{-2} year K^{-1} between the NCEP reanalysis and HadCRUT4 (Fig. S2B) with a central estimate of 12$\pm$3 W m^{-2} year K^{-1}, or 90$\pm$30 meters of equivalent ocean depth[1]. We note that the maximum value of C determined from any specific 10 year period in all temperature data sets is 150m equivalent ocean depth which sets an upper bound on the radiative e-folding timescale (τ) of 15 years, given our estimates of λ_{SW} and λ_{LW}.

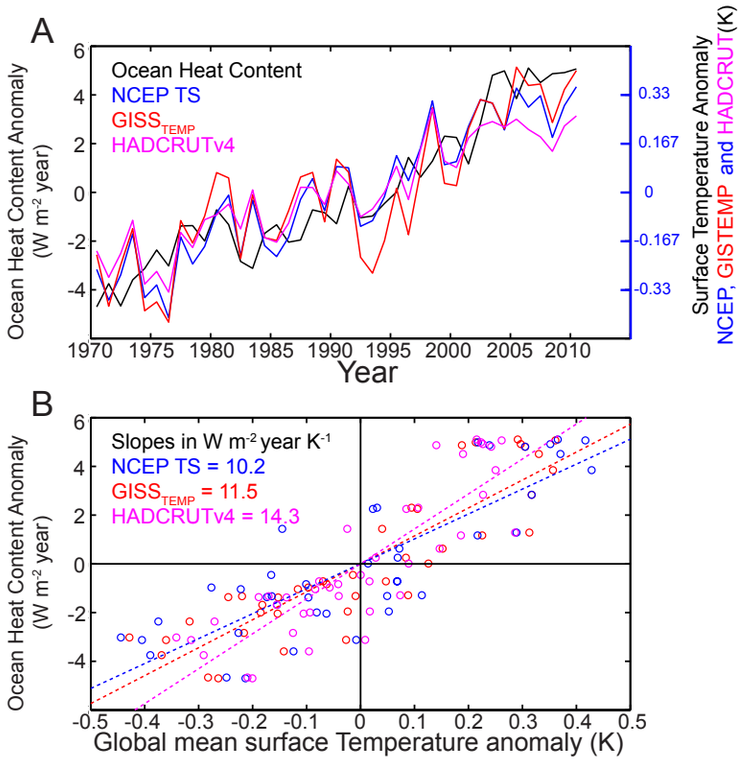

Fig. 2. (A) Time series of global ocean heat content anomaly (black– left axis) and global mean surface temperature anomaly (right axis) from NCEP reanalysis (blue), GISSTEMP (red) and Hadley Centre (purple). (B) Scatter plot of heat content and surface temperature anomaly. Each circle is an annual average anomaly and the dashed line is the linear best fit which represents the climate system heat capacity (values given in the legend). 1 W m^{-2} year K $^{-1}$ equals 7.6 meters of equivalent ocean depth.

1. Kim, K, North, G, & Huang, J. (1992) J. Geophys. Res. 97, 10069–10081.
2. Loeb, N. G, Wielicki, B. A, Doelling, D. R, Smith, G. L, Keyes, D. F, Kato, S, Manalo-Smith, N, & Wong, T. (2009) J. Climate 22, 748–766.
3. Donohoe, A & Battisti, D. (2011) J. Climate 24, 4401–4417.
4. Solomon, S, Daniel, J, Neely, R, Vernier, J.-P, Dutton5, E, & Thomason, L. (2011) Science 333, 866–870.
5. Hansen, J. e. a. (1992) J. Geophys. Res. 110, D18104.
6. Masarie, M. P. T. (1995) J. Geophys. Res. 100, 11593–11610.
7. Kalnay, E, Kanamitsu, M, Kistler, R, Collins, W, Deaven, D, Gandin, L, Iredell, M, Saha, S, White, G, Woollen, J, Zhu, Y, Leetmaa, A, Reynolds, B, Chelliah, M, Ebisuzaki, W, Higgins, W, Janowiak, J, Mo, K. C, Ropelewski, C, Wang, J, Jenne, R, & Joseph, D. (1996) Bull. Amer. Meteor. Soc.
8. Hansen, J, Ruedy, R, Glascoe, J, & Sato, M. (1999) J. Geophys. Res. 104, 30997–31022.
9. Cowtan, K & Way, R. (2014) Quart. J. Roy. Meteor. Soc.
10. Morice, C. P, Kennedy, J, Rayner, N, & Jones, P. (2012) J. Geophys. Res. 117, D08101.
11. Murphy, D, Solomon, S, Portmann, R, Rosenlof, K, & F.P.M. (2009) J. Geophys. Res. 114, D17107.

[1] An equivalent ocean depth is defined by the heat capacity of an ocean covering the entire surface area of the Earth.

12. Sveshnikov, A. (1979) Problems in probability theory, mathematics statistics and theory of random functions. (W.B Saunders Company).
13. Hartmann, D. (2014) Objective Analysis. (University of Washington).
14. Antonov, J, Levitus, S, Boyer, T, Conkright, M, OBrien, T, & Stephens, C. (1998).

Table 1. Estimates of radiative feedbacks using interannual regressions between forcing adjusted CERES EBAF radiation data and various surface temperature data sets. All values are in W m^{-2} K^{-1}. Uncertainties are assessed as one standard deviation of the regression coefficient uncertainty.

Temperature Data	λ_{SW}	λ_{LW}	λ
NCEP Reanalysis TAS	0.7 ± 0.4	-1.7 ± 0.2	-1.0 ± 0.3
GISTEMP	0.8 ± 0.4	-2.2 ± 0.3	-1.4 ± 0.4
CW HadCRUT4	0.9 ± 0.5	-2.0 ± 0.4	-1.1 ± 0.4
Average	0.8 ± 0.4	-2.0 ± 0.3	-1.2 ± 0.4